31st Congress of the International Council of the Aeronautical Sciences

Belo Horizonte, Brazil; September 09-14, 2018

USING SENSITIVITY PENALTIES TO ROBUSTIFY THE OPTIMAL REENTRY TRAJECTORY OF A HYPERSONIC VEHICLE

Tuğba Akman* , **Johannes Diepolder*** , **Benedikt Grüter*** , **Florian Holzapfel***

* **Institute of Flight System Dynamics, Technical University of Munich, Germany**

Keywords: *Trajectory Optimization, Reentry, Robust Optimal Control, Sensitivity Penalty, Aerothermodynamics*

Abstract

In the paper at hand, an optimal reentry trajectory for a winged hypersonic vehicle is calculated, where the maximum heat flux at the stagnation point is minimized. The main contribution of this paper is the robustification of the optimal reentry trajectory against air density fluctuations resulting in a robust trajectory, where the heat flux over the flight time is less sensitive against perturbations in air density. For this purpose, sensitivities describing the rate of change of the heat flux with respect to perturbations in air density are minimized. Solving the associated optimal control problem is based on direct solution methods, where the problem is discretized and solved as a finite dimensional optimization problem. The robustness is achieved by a two-step optimization. In the first optimization, the nominal problem, where the maximum heat flux is minimized, is to be solved. In the second optimization, high sensitivities are penalized by formulating a new cost function consisting of the sum of the maximum heat flux and weighted sensitivities resulting in robust optimal controls.

1 Introduction

High and long lasting thermal impact is critical for passengers and the overall structural integrity of the vehicle and also shortens the lifespan of the vehicle [1]. Factors that contribute to high heat flux are the vehicle shape [2] as well as environmental influences such as air density [3]. In [1, 3, 4], optimized trajectories with respect to constraints on heat flow at critical points and surfaces of the given vehicle can be found. Here, context and mission specific models are presented that serve as a basis for the optimal control problem which is to be solved.

Due to specific environmental conditions (e.g. time of day or weather) the air density at one and the same altitude can vary in time or measurements can contain errors [5]. The U.S. Standard Atmosphere [5] serves as a basis for many air density models used in literature [4, 6]. These assume a perfect air density without any disturbances and errors. To obtain a more realistic description of air density, uncertainties can be taken into account by modelling them as e.g. continuous deviations from the nominal air density profile [3].

A trajectory, that results from models, that do not take into account uncertainties, is called *nominal trajectory*. In contrast, a trajectory, that does not change a certain system output of interest significantly when parameter values are perturbed, is called *robust trajectory*. Influences of parameter changes on system outputs or on the trajectory can formally be expressed by the derivative of the output with respect to the parameter, the so called *sensitivity*.

The aim of this paper is to compute heat minimal reentry trajectories, that are robust against perturbations in air density, by introducing uncer-

tainties of air density and an extended cost function to be minimized that penalizes high sensitivities. The study is structured as follows: In section 2, the dynamic, aerodynamic, thermal and environmental models are presented. Section 3 presents the idea of direct optimal control theory. Section 4 describes the nominal and robust optimal control problem with sensitivity penalties. In section 5, the optimized nominal and robust reentry trajectories are calculated, discussed and compared. In section 6, a conclusion and an outlook follows.

2 Modelling

In this section, the model of the dynamic system, the aerodynamics, heat flux and air density based on [4, 3, 7] are described as they are used in the optimizations.

2.1 Dynamic Model

The state dynamics of the reentry vehicle are given by a point mass model with the following differential equations:

$$\dot{h} = V\sin(\gamma), \tag{1}$$

$$\begin{aligned}\dot{V} = &-\frac{D}{m} - g\sin(\gamma) + \omega_e^2(R_e+h)\cos(\lambda)\\ &\cdot(\sin(\gamma)\cos(\lambda) - \cos(\gamma)\sin(\chi)\sin(\lambda)),\end{aligned} \tag{2}$$

$$\begin{aligned}\dot{\gamma} = &\frac{L}{mV}\cos(\mu) - \left(\frac{g}{V} - \frac{V}{R_e+h}\right)\cos\gamma\\ &+ 2\omega_e\cos(\chi)\cos(\lambda)\\ &+ \omega_e^2\frac{R_e+h}{V}\cos\lambda\\ &\cdot(\sin(\chi)\sin(\gamma)\sin(\lambda) + \cos(\gamma)\cos(\lambda)),\end{aligned} \tag{3}$$

$$\begin{aligned}\dot{\chi} = &\frac{L}{mV\cos(\gamma)}\sin(\mu) - \frac{V}{R_e+h}\cos(\gamma)\cos(\chi)\\ &+ \tan(\lambda) + 2\omega_e(\sin(\chi) + \cos(\lambda)\tan\gamma - \sin(\lambda))\\ &- \omega_e^2\frac{R_e+h}{V\cos(\gamma)}\cos(\lambda)\sin(\gamma)\cos(\chi),\end{aligned} \tag{4}$$

$$\dot{\lambda} = \frac{V\cos(\gamma)\cos(\chi)}{(R_e+h)\cos(\lambda)}, \tag{5}$$

$$\dot{\varphi} = \frac{V\cos(\gamma)\sin(\chi)}{R_e+h}, \tag{6}$$

where h is the altitude, V the velocity, γ the flight path angle, χ the course angle, μ the bank angle and λ and φ are the longitude and latitude, respectively. The lift and drag forces are denoted by L and D. The altitude dependent gravitational model is described by

$$g(h) = g_0\left(\frac{R_e}{R_e+h}\right)^2$$

with gravitational acceleration $g_0 = 9.8067\,\mathrm{m/s^2}$. The vehicle's mass is given by $m = 115\,000\,\mathrm{kg}$. The earth's rotational velocity is given by $\omega_e = 7.2921\times10^{-5}\mathrm{rad/s}$ and the earth radius by $R_e = 6371\,\mathrm{km}$.

2.2 Air Density

The air density as described by the US Standard atmosphere [5] is modelled by a smooth exponential function [4]:

$$\begin{aligned}\rho(h) = \exp\Bigg(&\frac{c_1h^5 + c_2h^4 + c_3h^3 + c_h^2 + c_5h + c_6}{c_7h^3 + c_8h^2 + c_9h + c_{10}}\\ &+ \cos(c_1h^{d_2} + d_3)\frac{d_4}{d_5h + d_6}\\ &- e_1\exp\left(e_2(h-e_3)^2\right)\Bigg)\end{aligned} \tag{7}$$

for altitudes up to 200 km. For the coefficients c, d please refer to [4].

2.3 Thermal Model

The convective heat flux $\dot{q}$ at the stagnation point is described by [2]

$$\dot{q} = K_e\left(\frac{\rho}{R_n}\right)^{1/2}v^3, \tag{8}$$

where $K_e = 5.199111\times10^{-5}\ (\mathrm{kg/m^2})^{1/2}$ is an atmosphere specific constant and $R_n = 4\,\mathrm{m}$ is the nose radius of the vehicle.

2.4 Aerodynamic Model

The lift and drag are modelled by

$$L(h,V,C_L) = p(V,h)\ F\ C_L, \tag{9}$$
$$D(h,V,C_L) = p(V,h)\ F\ C_D(C_L), \tag{10}$$

where the reference area is given by $F = 305\,\mathrm{m}^2$. Air pressure p and the drag coefficient C_D are calculated by

$$p(v,h) = \frac{1}{2}\rho(h)v^2 \tag{11}$$
$$C_D(C_L) = C_{D_0} + k\ {C_L}^2 \tag{12}$$

with lift coefficient C_L and coefficients $C_{D_0} = 0.017$ and $k = 2$ depending on the flight system's configuration.

3 Applied Optimal Control

The aim of optimal control is to find a control history, that minimize a given cost function. Let n_u be the number of controls, n_x the number of states and n_p be the number of parameters. A common optimal control problem can be stated as follows [8, 9]:

Minimize the *Bolza cost functional*

$$J = e(\mathbf{x}(t_f),\mathbf{u}(t_f),\mathbf{p},t_f) + \int_{t_0}^{t_f} L(\mathbf{x}(t),\mathbf{u}(t),\mathbf{p},t)\ dt \tag{13}$$

by determining the optimal control histories $\mathbf{u}$ with $\mathbf{u}\colon [t_0,t_f] \to \mathbb{R}^{n_u}$, the optimal state histories $\mathbf{x}$ with $\mathbf{x}\colon [t_0,t_f] \to \mathbb{R}^{n_x}$ and the optimal parameters $\mathbf{p} \in \mathbb{R}^{n_p}$ subject to the state dynamics

$$\dot{\mathbf{x}}(t) = \mathbf{f}(\mathbf{x}(t),\mathbf{u}(t),\mathbf{p}), \tag{14}$$

model output equation

$$\mathbf{y}(t) = \mathbf{g}(\mathbf{x}(t),\mathbf{p}) \tag{15}$$

for all $t \in [t_0,t_f]$, the initial and final boundary conditions

$$\psi(\mathbf{x}(t_0),\mathbf{x}(t_f)) = \mathbf{0} \tag{16}$$

and the equality and inequality constraints

$$\mathbf{c}_{eq}(\mathbf{x}(t),\mathbf{u}(t),\mathbf{p},t) = \mathbf{0}, \tag{17}$$
$$\mathbf{c}_{ineq}(\mathbf{x}(t),\mathbf{u}(t),\mathbf{p},t) \leq \mathbf{0} \tag{18}$$

for all $t \in [t_0,t_f]$.

In practical applications, the cost function and the constraints refer to context and mission specific models. The models in section 2 correspond to equality constraints. Inequality constraints can be any kind of bound for a state or control, e.g. an altitude constraint stating that the altitude must not exceed a certain value.

When solving an optimal control problem, either function space methods or transcription approaches can be applied [8, 9]. In function space methods, the optimal control problem is considered as an infinite dimensional optimization problem in a suitable function space. Here, optimization algorithms are directly applied to the infinite optimization problem. In contrast, transcription approaches aim to discretize the optimal control problem and transfer it to a finite dimensional optimization problem. Here, optimization methods are applied to the finite dimensional optimization problem. For the evaluation of the differential equation restrictions numerical solvers based on e.g. Runge Kutta techniques are utilized. Common discretization techniques are single shooting, multiple shooting and collocation [8, 9]. The method used here is collocation, where every discretized time step of the states and controls is contained in the optimization vector.

4 Sensitivity Penalty

The major task in solving problem (13) - (18) is to find a solution that fulfills the flight system dynamics, i.e. the underlying differential equations. Since these may not be unique and differ with parameter perturbations, the optimal system outputs depending on the states may strongly be affected by parameter perturbations. This dependency can be measured by sensitivities describing the rate of change of the system outputs with respect to perturbations of parameters.

The sensitivity $S_{\mathbf{y}}$ of the system outputs $\mathbf{y}$ in equation (15) with respect to parameters $\mathbf{p}$ is defined by [8]:

$$S_{\mathbf{y}}(t) = \frac{\partial \mathbf{g}(\mathbf{x}(t), \mathbf{u}(t), \mathbf{p}(t))}{\partial \mathbf{p}}. \tag{19}$$

A robust optimal trajectory is defined as a trajectory, where system outputs do not change significantly when perturbing a parameter. The aim of the robust optimization in section 5.3 is to both minimize J and $S_{\mathbf{y}}$ at the same time. Optimization methods that minimize more than one cost function are e.g. multi-criteria optimization methods [10] or bi-level methods [6].

The robust optimization approach in this paper is as follows: In order to keep the sensitivity $S_{\mathbf{y}}$ small, its weighted norm is minimized together with the cost function J. This gives rise to a robust optimal control problem:

$$\text{minimize} \quad J + \int_{t_0}^{t_f} \| S_{\mathbf{y}}(t)^T A(t) S_{\mathbf{y}}(t) \| \, dt \tag{20}$$

with constrains from section 3. Here, the diagonal matrix $A(t) \in \mathbb{R}^{n_p}$ contains the weights for each parameter sensitivity and $\|\cdot\|$ defines a suitable norm.

This can be seen as a multi-criteria optimization problem. Another way to interpret the cost function (20) is that the squared sensitivities $S_{\mathbf{y}}^T A S_{\mathbf{y}}$ are penalized. The higher the weights in A the greater the penalty.

The sensitivity matrix $S_{\mathbf{y}}$ can be calculated by

$$S_{\mathbf{y}} = \frac{\partial \mathbf{g}}{\partial \mathbf{p}} + \frac{\partial \mathbf{g}}{\partial \mathbf{x}} \cdot \frac{\partial \mathbf{x}}{\partial \mathbf{p}} \tag{21}$$

The first parts, $\frac{\partial \mathbf{g}}{\partial \mathbf{p}}$ and $\frac{\partial \mathbf{g}}{\partial \mathbf{x}}$, can be computed analytically. The part $\frac{\partial \mathbf{x}}{\partial \mathbf{p}}$ describes the sensitivity of the states $\mathbf{x}$ with respect to parameters $\mathbf{p}$. Here, it is denoted by $S_{\mathbf{x}}$ and can be calculated by solving the sensitivity differential equation [8]:

$$\begin{aligned} \dot{S}_{\mathbf{x}}(t) &= \frac{\partial \mathbf{f}(\mathbf{x}(t), \mathbf{u}(t), \mathbf{p}(t))}{\partial \mathbf{x}} \cdot S_{\mathbf{x}}(t) \\ &\quad + \frac{\partial \mathbf{f}(\mathbf{x}(t), \mathbf{u}(t), \mathbf{p}(t))}{\partial \mathbf{p}}, \\ S_{\mathbf{x}}(t_0) &= \mathbf{x}(t_0). \end{aligned} \tag{22}$$

For numerical computation, $S_{\mathbf{x}}$ is defined as an additional state in the optimization problem (13)-(18) fulfilling the differential equation (22) and can then be computed simultaneously with the other states $\mathbf{x}$. A similar approach can be found in [11].

5 Numerical Results

For the nominal trajectory, the reentry problem is solved with unperturbed parameters in the following scenario: Minimize the parameter $\dot{q}_{max}$ that represents the maximum heat flux value, such that

$$\dot{q}(t) \leq \dot{q}_{max} \tag{23}$$

for all $t \in [t_0, t_f]$, by determining optimal controls, namely the lift coefficient

$$C_L \in [0.1, 0.18326]$$

and the bank angle

$$\mu \in [-\pi/2, \pi/2].$$

The bounds on the states are set to

$$\begin{aligned} h &\in [0, 200000] \text{ m} \\ V &\in [0, 8000] \text{ m/s} \\ \gamma &\in [-\pi, \pi] \text{ rad} \\ \chi &\in [-\pi, \pi] \text{ rad} \\ \lambda &\in [-\pi/2, \pi/2] \text{ rad} \\ \varphi &\in [-\pi, \pi] \text{ rad} \\ q &\in [0, \infty) \text{ J/m}^2 \end{aligned}$$

The initial and final boundary conditions are given by

State	t_0	t_f
h [m]	120×10^3	24×10^3
V [m/s]	7000	80
γ [rad]	0	-
χ [rad]	-0.659	-
λ [rad]	-	0.192
φ [rad]	-	0.83778
q [J/m^2]	0	-

Please note that there are no initial boundaries set for the position due to the fact that these are also supposed to be optimized. The starting position of the vehicle influences the optimal solution due to influences on e.g. range or flight time. The increase in heat flux is negligible when manoeuvring to the starting position in the lower earth orbit. Therefor, the starting velocity is fixed. Furthermore, the load factor $n_z = \frac{L}{mg}$ is constrained to the interval $[-1, 2.5]$. The optimization is performed with the optimal control tool FALCON.m [12].

5.1 Nominal Optimization Results

The nominal optimal trajectories and controls are depicted in figure 1 and figure 2, respectively, by black lines.

In the first phase, the vehicle descends at a steep angle until an altitude of 54 km, where air density increases faster and the maximum heat flux value is reached, before it descends at a smaller angle until an altitude of 40 km. Afterwards, it performs skips that become more and more shallow until the final boundary conditions are met. The heat flux peak is reached at a value of 2.1699×10^6 m/s^2 and is hold constant for 430 s while the shallow reentry phase.

In figure 3, the sensitivities $(\frac{\partial \dot{q}}{\partial \delta})^2$ are presented. The heat flux is highly sensitive to air density fluctuations before the skip at an altitude of 40 km, where air density increases and where the maximum heat flux value is reached.

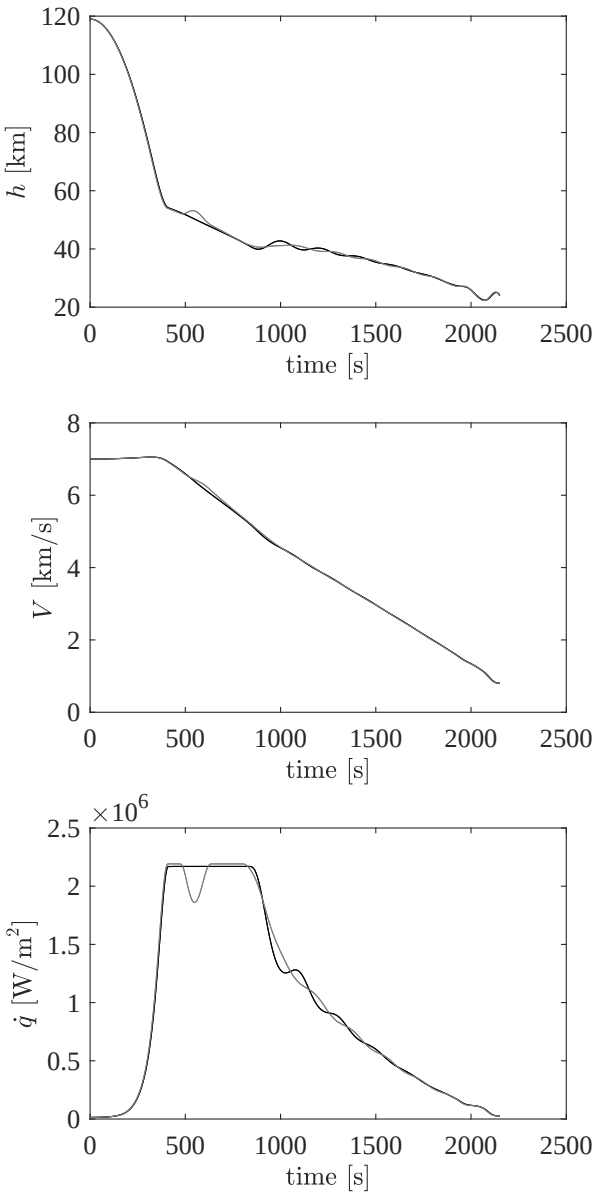

Fig. 1 Nominal (black line) and robust (grey line) optimal states h and V and state derivative $\dot{q}$.

5.2 Simulation

The parameter perturbation in air density is linearly modelled by

$$\rho_\delta(h) = (1+\delta)\rho(h) \tag{24}$$

with the perturbation parameter $\delta \in [-0.1, 0.1]$ describing the deviation from the nominal value $\rho(h)$ up to 10%. The trajectories of the heat flux are simulated with 20 equidistant values for $\delta \in [-0.1, 0.1]$ with the nominal optimal controls from section 5.1. The impact of air density perturbations on the heat flux profile is illustrated in figure 4. In the simulations with $\delta \neq 0$, the maximum heat flux value is not constant over a time period but deviates strongly in the region, where the nominal heat flux reaches its peak. The maximum value of the heat flux differs up to 5.47% from the nominal one.

5.3 Robust Optimization

The approach for the robust optimization is to minimize the penalized cost function (20). The

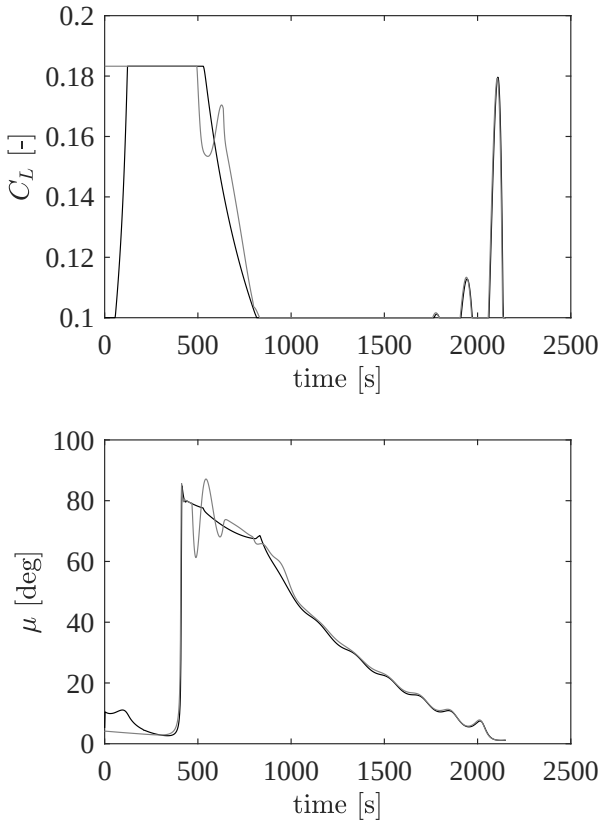

Fig. 2 Nominal (black line) and robust (grey line) optimal controls C_L and μ.

sensitivity penalty term is chosen to be

$$S_{\mathbf{y}}(t)^T A(t) S_{\mathbf{y}}(t) = 10^{-9} \cdot \frac{\dot{q}(t)}{\dot{q}_{max}} \cdot \left(\frac{\partial \dot{q}}{\partial \delta}(t) + S_{\mathbf{x}}(t) \frac{\partial \dot{q}}{\partial \mathbf{x}}(t) \right)^2, \quad (25)$$

The first weight 10^{-9} is introduced such that $\dot{q}_{max}$ and $S_{\mathbf{y}}$ have the same order of magnitude. The weight $\frac{\dot{q}}{\dot{q}_{max}}$ penalizes high values of $\dot{q}$ more than smaller values. Furthermore, the path constraint

$$\dot{q}(t) \leq 1.01 \cdot \dot{q}^*_{max} \quad (26)$$

for $\dot{q}$ is introduced, which is based on the nominal optimal heat flux peak $\dot{q}^*_{max}$ in order to assure that the robust heat flux peak does not deviate from the nominal one more than one percent. This yields the robust optimal trajectories as depicted in figure 1 and figure 2 in grey lines. In this case, the heat flux peak is reached at a value of $2.1916 \times 10^6 \mathrm{W/m^2}$, which is a deviation of

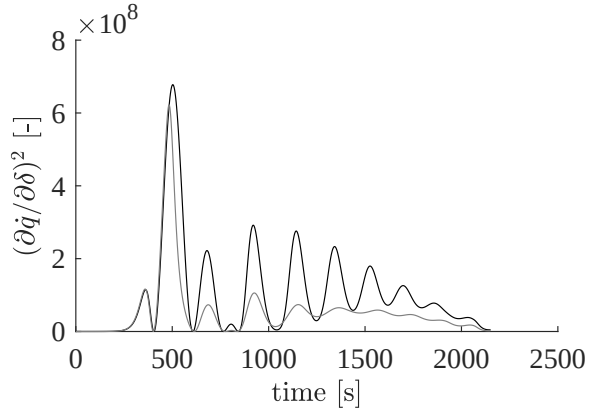

Fig. 3 Sensitivities $(\partial \dot{q}/\partial \delta)^2$ of heat flux with respect to air density fluctuations over time of the nominal (black) and robust (grey) optimal trajectories.

1% of the nominal heat flux peak. Similar to the nominal trajectory, a skip glide is performed. Here, an additional skip at an altitude of 53 km is performed, which can be explained by the fact that the air density decreases at higher altitudes leading to a non-increasing heat flux.

On the right hand side of figure 4, the simulated profile of the heat flux for air density perturbations as described in section 5.2 is depicted. The maximum value for the heat flux is perturbed up to 5.05%. When comparing the sensitivities from the nominal and robust solution in figure 3, one can see that over the whole time span, the sensitivities of the robust solution (black line) are smaller than the sensitivities of the nominal solution (grey line). Hence, the deviations from the robust optimal heat flux are smaller than in the nominal case, when air density is perturbed. Furthermore, we can see that the sensitivities are the highest where the maximum heat flux is reached and at altitudes around 40 km, where air density increases faster.

6 Conclusion and Outlook

A robust heat minimal reentry trajectory is computed, where the maximum heat flux is less sensitive against air density fluctuations. In the presented robust optimization approach high sensitivities of the heat flux describing the dependency

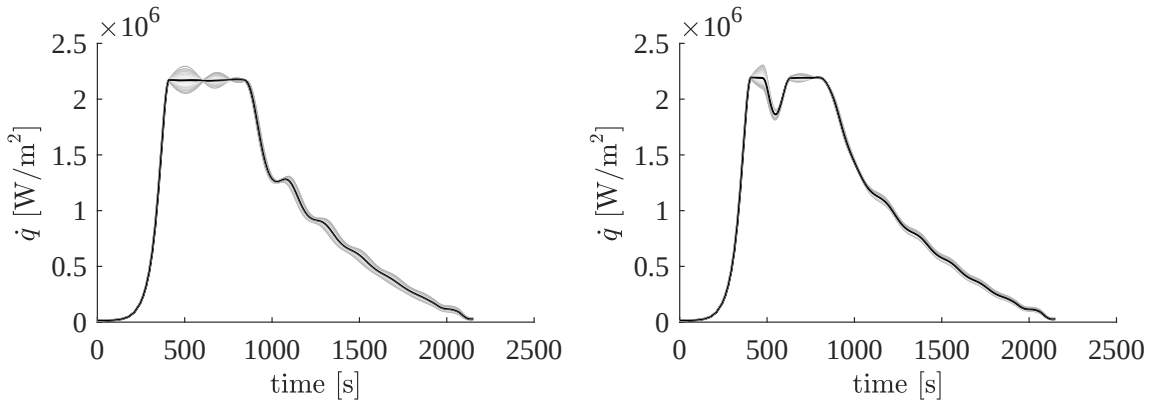

Fig. 4 Simulation of heat flux after parameter perturbations with nominal controls. The black line represents the nominal heat flux, where the grey lines are simulation results with the respective optimal controls for parameter perturbations up to 10%.

of the heat flux from air density fluctuations are penalized. The resulting robust trajectory performs a skip reentry, where air density starts to have significant impact on the heat flux, namely, where the heat flux reaches its maximum.

In this work, one uncertain parameter was considered. For future work, a multidimensional uncertain parameter vector could be considered, which increases the problem size. Since the computation effort for the collocation of the sensitivities might be too high, one might consider computing the sensitivities by shooting methods. Furthermore, the uncertainty models can be reformulated by taking into account that at higher altitudes uncertainty in air density is higher. Also, the vehicle model and especially the thermal model can be extended, such that the obtained results reflect more realistic trajectories.

7 Contact Author Email Address

Tuğba Akman: tugba.akman@tum.de

References

[1] Dinkelmann, M. *Reduzierung der thermischen Belastung eines Hyperschallflugzeugs durch optimale Bahnsteuerung*, Dissertation, Technische Universität München, 1997.

[2] Sutton, K., and Graves Jr, R. A. *A general stagnation-point convective heating equation for arbitrary gas mixtures*, National Aeronautics and Space Administration, Washington, DC, 1971.

[3] Pescetelli, F., Minisci, E., and Brown, R. E. *Reentry trajectory optimization for a SSTO vehicle in the presence of atmospheric uncertainties*, 5th European Conference for Aeronautics and Space Sciences (EUCASS), 2013

[4] Mayrhofer, M. *Verbesserung der Missionssicherheit eines zukünftigen zweistufigen Raumtransportsystems mittels Flugbahnoptimierung*, Dissertation, Technische Universität München, 2002.

[5] U. S. Standard Atmosphere. *US standard atmosphere 1976.*, US Government Printing Office, Washington, DC, 1976.

[6] Richter, M., Bittner, M., Rieck, M. and Holzapfel, F. *A non-cooperative bi-level optimal control problem formulation for noise minimal departure trajectories*, 29th Congress of the International Council of the Aeronautical Sciences (ICAS), pp 7-12, 2014.

[7] Büskens, C. and Gerdts, M. *Emergency Landing of a Hypersonic Flight System: A Corrector Iteration Method for admissible Real-Time Optimal Control Approximations*, Optimalsteuerungsprobleme in der Luft-und Raumfahrt, Workshop in Greifswald of the special research project 255, 2003.

[8] Gerdts, M. *Optimal control of ODEs and DAEs*, Walter de Gruyter, 2012.

[9] Betts, J. T. *Practical methods for optimal control and estimation using nonlinear program-*

ming, Vol. 19, Siam, 2012.

[10] Hillermeier, C. *Nonlinear Multiobjective Optimization*, Birkhäuser Basel, Basel, 2001.

[11] Loxton, R. and Teo, K. L. *Robust suboptimal control of nonlinear systems*, Applied Mathematics and Computation, Vol. 14, Nr. 217, pp 6566-6576, 2011.

[12] Rieck, M., Bittner, M., Grüter, B., Diepolder, J. and Piprek, P. *FALCON.m User Guide*, www.falcon-m.com, 2017.

Copyright Statement